Environ Geol (2007) 52:27–40
DOI 10.1007/s00254-006-0446-3

ORIGINAL ARTICLE

Characterization of land subsidence induced by groundwater withdrawals in Su-Xi-Chang area, China

Xiao-Qing Shi · Yu-Qun Xue · Shu-Jun Ye · Ji-Chun Wu · Yun Zhang · Jun Yu

Received: 19 March 2006 / Accepted: 18 July 2006 / Published online: 8 August 2006

Abstract Su-Xi-Chang area is one of the typical regions in China which suffers from severe land subsidence. Various tools of field monitoring were integrated to study the characteristics and mechanisms of land subsidence in this region. The occurrence and the development of the land subsidence in this region are strongly related to the groundwater pumping both in time and space. The main consolidation layers are the soft mud layers; however, the compressibility of the confined sandy layers should not be ignored. The second and third confined aquifers contributed more than 30% of total subsidence. Meanwhile, irrecoverable deformations were also observed in the sandy layers. Different sandy layers deform diversely under different stress conditions. Some have the elastic feature. But the soil strata, including both sandy layers and clayey layers, located in the center of the groundwater level depression cone exhibited obvious viscous mechanical behavior which caused the common lag phenomenon. The sand composition (mingled with small clay particles or interbeds) and sand rheology are the two main reasons for the lag phenomena in sandy layers. A series of laboratory tests for modeling the effective stress changes due to groundwater withdrawals, were conducted to investigate the mechanism of the lag phenomenon. Based on the test results, the relationship of stress–strain–time for saturated sands is obtained; and it could be expressed as power functions. The results also showed that the compression of the sandy layers was time dependent, and its deformation could be remarkable. When establishing land subsidence model, the deformation for the similar soil formation could be elastic, visco-elastic and even visco-elastic–plastic, because of the different groundwater level fluctuation experienced.

Keywords Land subsidence · Lag phenomenon · Sandy layer · Creep · Su-Xi-Chang area

X.-Q. Shi (✉) · Y.-Q. Xue · S.-J. Ye · J.-C. Wu · Y. Zhang
Department of Earth Sciences, Nanjing University,
Nanjing, China
e-mail: shixiaoqing@nju.org.cn

J. Yu
Geological Survey of Jiangsu Province,
Nanjing, China

Introduction

Land subsidence due to excessive withdrawal of groundwater has become a worldwide problem. Many countries or districts have encountered this costly geological hazard (USGS 1999) and this problem has been extensively investigated both quantitatively and qualitatively by previous researchers (Pratt and Johnson 1926; Poland and Davis 1969). Previous studies concluded that a key to the problem of land subsidence was the correct evaluation of the behavior of clay layers (aquitards) (Helm 1975, 1976; Gambolati and Freeze 1973; Gambolati et al 1974). As a result, the deformation of sandy layers (aquifers) was usually ignored and underestimated. LEHGGS and GCSER (1989) investigated the land subsidence of the urban of Shanghai and proposed a predictive model to calculate the land subsidence. In their model, the sandy layers were assumed to be of a linear elastic nature and the behavior of clay layers obeyed Terzaghi's one dimensional consolidation theory. This assumption was also used in many other researches (Hu 2002; Leake 1990;

Sneed and Galloway 2000). Men (1999a, b) and Gu and Ran (2000) studied the creep deformation of shallow soft clay layers 1 and 2 in Shanghai by laboratory tests. They concluded that the soft clay had a creep behavior and it should be considered in the calculation of land subsidence; however, the deformation of sandy layer was still underestimated. Unfortunately, this is not always the case that the problem of land subsidence laid on the compressibility of the aquitards. Liu et al. (2004) found that irrecoverable volumetric strains were observed in the sandy layers in the Choshui River alluvial fan, Taiwan. It is shown that the characterization of the soil strata deformation varies from region to region because of complicated soil formations and groundwater withdrawal. The compression of the soil stratum caused by the change of groundwater level is complicated and has not been understood comprehensively.

Su-Xi-Chang area (including Suzhou, Wuxi and Changzhou Cities), located together at the lower reaches of the Yangtze River in the southern Jiangsu Province of China, is one of the typical regions which are suffering from the increasingly severe land subsidence caused by extensive groundwater exploitation. By the end of the last century, the accumulative subsidence was over 1 m in Su-Xi-Chang area and the maximum was more than 2 m.

The land subsidence in Su-Xi-Chang area is complicated and has some unique characteristics because of its pumping conditions and soil formations. This aim of this paper has been to study the characteristics, patterns and mechanisms of land subsidence in this region. This will be helpful for constructing the mathematic model of land subsidence in the future.

Geographical location and hydrogeology of Su-Xi-Chang area

Su-Xi-Chang area is located in the southeast of the Jiangsu Province. It stretches from Changzhou on the west and to Shanghai on the east. It borders the Yangtze River on the north and is separated from the Zhejiang Province on the south by the Tai Lake. The total area is 17,510 km^2, including Suzhou, Wuxi, Changzhou cities and other 12 counties. Figure 1 shows the geographical location of Su-Xi-Chang area.

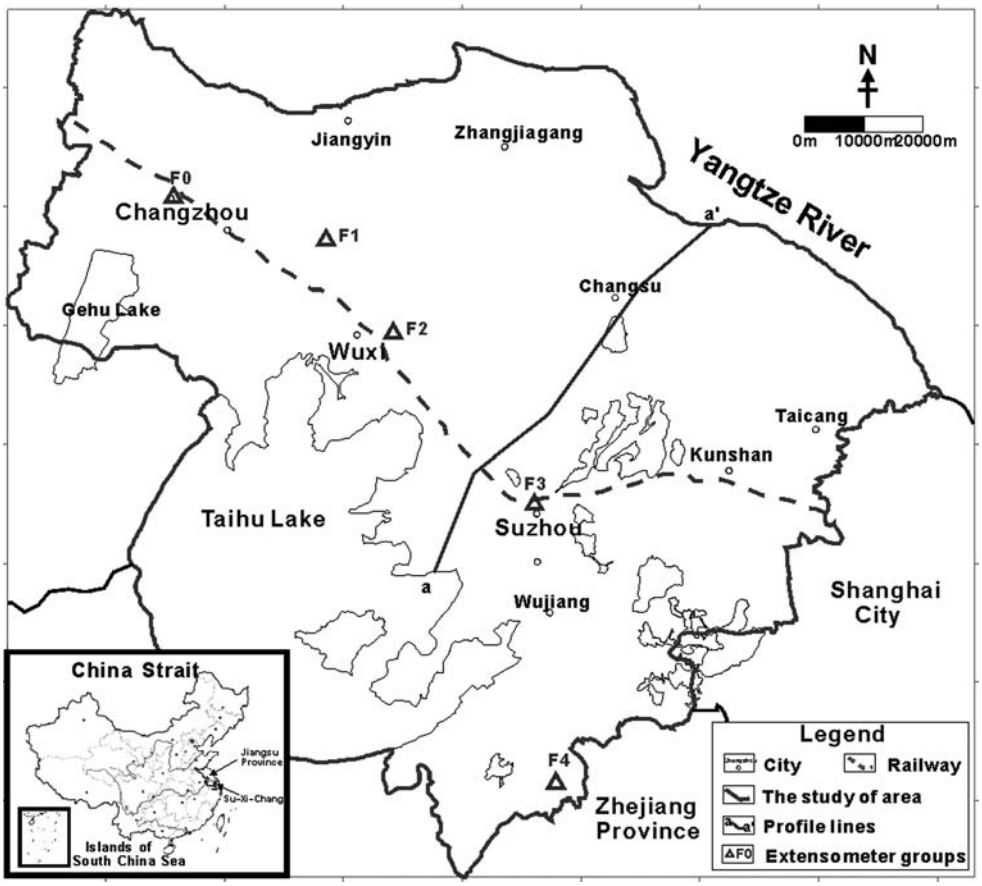

Fig. 1 Geographical location of Su-Xi-Chang area in China

This region lies in the lower Yangtze River alluvial plain and the average elevation is less than 6 m. The Quaternary strata are widely distributed and the deposit thickness increases from west to east and from south to north. Based on sedimentological data, together with evidence from the study of soil properties, the aquifer system consist of the inter-layering of four aquifers, including one unconfined aquifer and three confined aquifers and four aquitards. Figure 2 presents the hydrostratigraphy along a cross-section line in Su-Xi-Chang area.

Groundwater pumping and land subsidence

With the rapid development of the economy and the severe pollution of surface water in Su-Xi-Chang area, the usage amount of groundwater is gradually increased. Overpumping from the aquifers results in a significant drop of the groundwater level, which caused an increase in effective stress and led to the consolidation of sedimentary deposits. In addition, the compressible strata and complex soil formations in this region provide the internal condition for land subsidence.

The land subsidence in this region was first discovered in the 1960s. Before the 1980s, the groundwater pumping focused on three central cities: Suzhou, Wuxi and Changzhou. Thus the subsidence took place in the centers. After 1990s, the groundwater was pumped all over the area and the subsidence spread to the whole area. The configuration of the subsidence cone in some places, such as the downtown of Suzhou and Changzhou and the west of Wuxi, is basically identical with the shape of the groundwater depression cone. Figure 3 presents the evolution of groundwater depression cone of the main pumping aquifer (second confined aquifer) and land subsidence depression cone. There were strong relationships between the development of land subsidence and the groundwater level of the main pumping aquifer.

In the view of one single city, the observational data of the groundwater yield, groundwater level of the main pumping aquifer and the subsidence of Suzhou City from 1982 to 2000 (Fig. 4) illustrate that the subsidence change trend is consistent with the yield trend. In the period from 1984 to 1987, the yield increased annually and the annual subsidence increased. The maximum annual subsidence was 90 mm. After 1988, the groundwater yield decreased and the annual subsidence decreased gradually. Especially after 1995, the yearly subsidence has been controlled in 30 mm. As demonstrated in the Fig. 5, the situation in Changzhou City is the same as that in the Suzhou. Notable, the groundwater level of the main pumping aqufier in both of the cities increased obviously with the decrease of

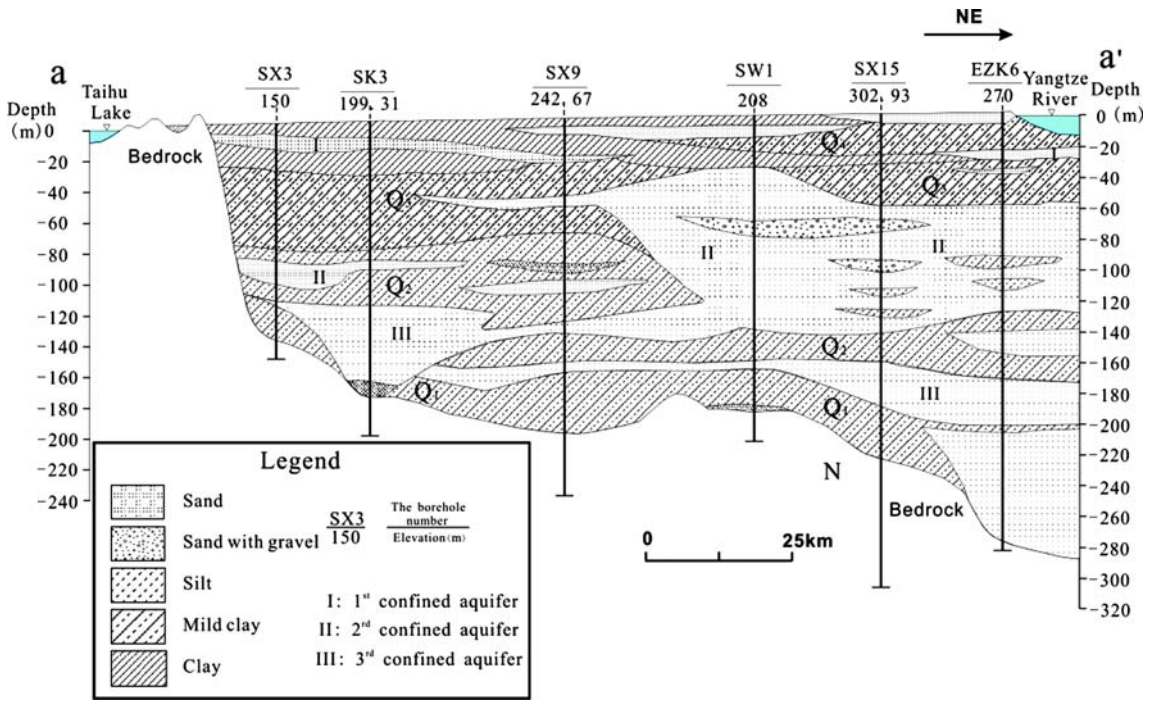

Fig. 2 Hydrostratigraphy along the cross-section line a–a′ of Su-Xi-Chang area. *Profile lines* are indicated in Fig. 1

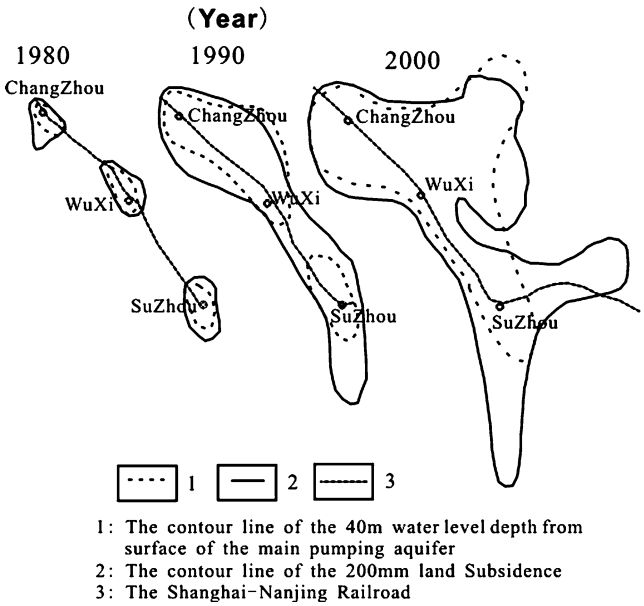

Fig. 3 Sketch contour map of accumulated ground settlement (in mm) based on the survey in 1980–2000 (modified from Yu et al. 2004)

groundwater pumping after 1995. However, the land subsided continually just as showed in Figs. 4 and 5. This problem would be deeply discussed in the next section.

The features of land subsidence

The preliminary analysis showed excessive groundwater withdrawal is the main reason of the land subsidence in Su-Xi-Chang area. There are 5 extensometer groups and more than 100 observation wells in Su-Xi-Chang area. These extensometer groups and observation wells provide an invaluable historical record of deformation and pore-water pressure, and make it convenient to investigate the special features of soil deformation when the groundwater level changes due to pumping.

The F0 extensometer, located in the center of groundwater depression cone in Changzhou, is the one that has the longest series of observational data of land

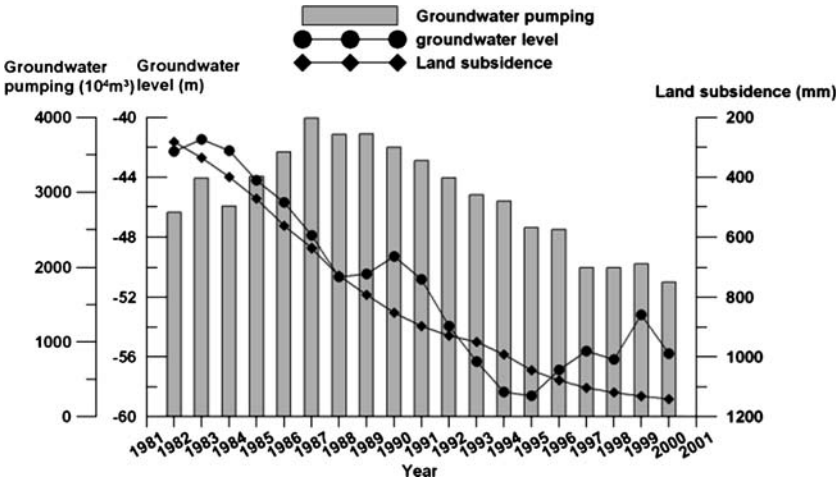

Fig. 4 The curves of groundwater pumping, groundwater level of main pumping aquifer and land subsidence in Suzhou City (1982–2000)

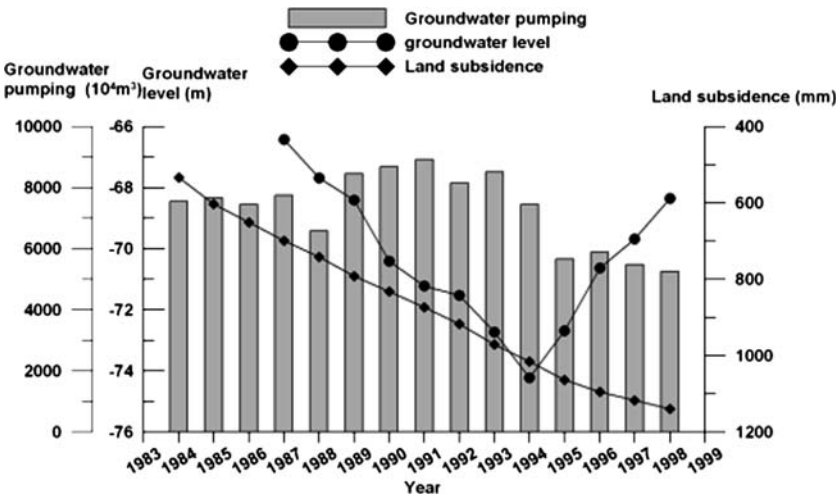

Fig. 5 The curves of groundwater pumping, groundwater level of main pumping aquifer and land subsidence in Changzhou City (1984–1998)

subsidence. The other four extensometers, located in the depression cone of other cities, were built lately and have a short series of observation data. Therefore, the data from the F0 extensometer were analyzed to investigate the compression deformation contributed by various individual layers.

Figure 6 presents the histogram of the geological borehole and the variation of the clay content (grain size <0.005 mm) with the depth of F0 extensometer. As Fig. 6 demonstrates, because of the complicated geological condition in field, the sandy layer formation is complicated. It is not always composed of pure sand but is perhaps mingled with small clay particles or interbeds in sandy layer, such as the third confined aquifer. However, for the second confined aquifer, there was little clay particles or interbeds. Note the different compostition for the second and third confined aquifers, which is important to analyze the special features of individual layer deformation in the next section.

Figure 7 presents the ratio of compression deformation in layers at different depths, which indicates the second and third confined aquifers and the second aquitard contributed more than 90% of total subsidence in the period from 1984 to 2001. The clay layers above the second confined aquifer, especially the clay layers whose water level depth from the surface is 35.40–92.80 m, are the main consolidation layer. The ratio of compression deformation for these clay layers is 57.15%. The compaction subsidence is in direct ratio with the thickness of the clay layer. For the clay layer

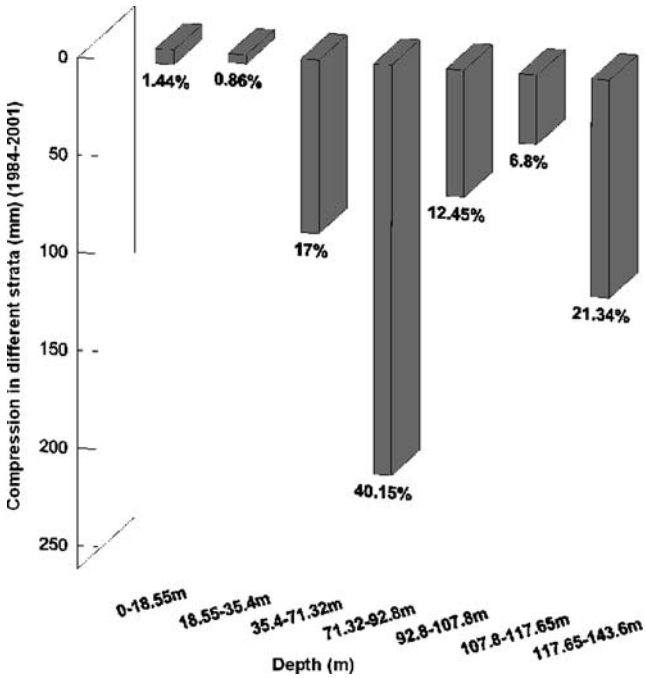

Fig. 7 Ratio of compression deformation for individual layer at different depths in F0 extensometer (there is lack of first aquitard. *Positive value* stands for compression, and *negative* stands for extension hereafter)

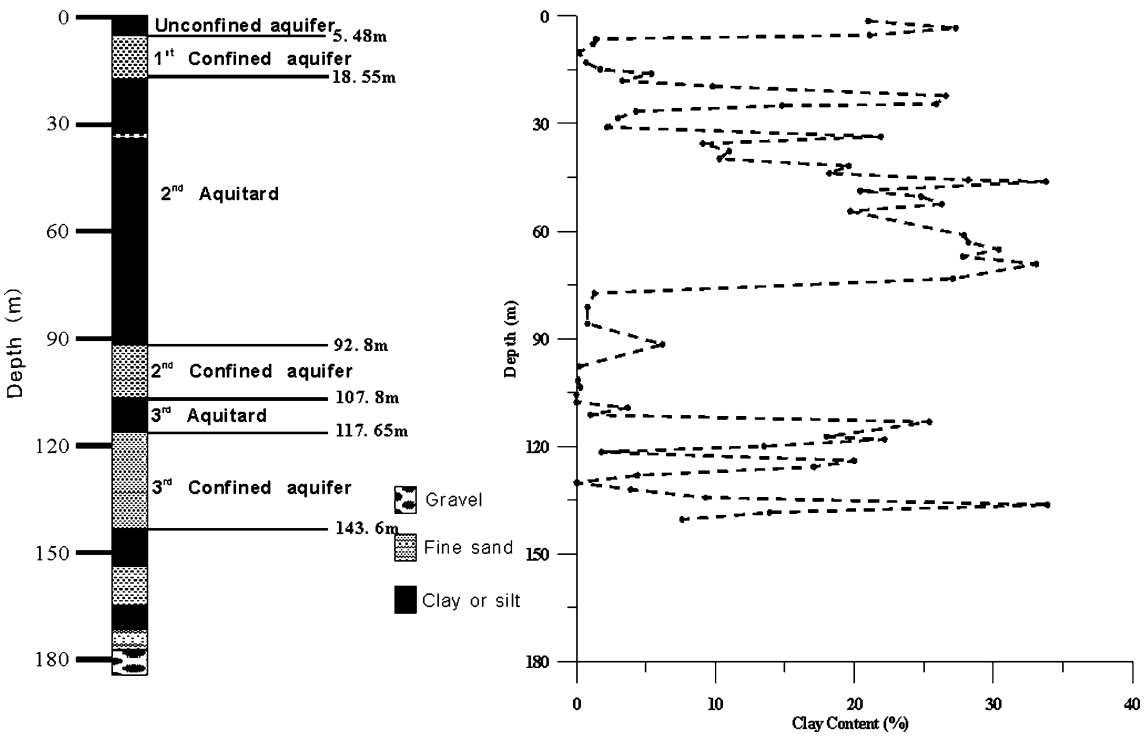

Fig. 6 The histogram of the geological borehole and the variation of the clay content with the depth of F0 extensometer

with the unit thickness, the more close to the pumping aquifer, the larger of the subsidence of the unit thickness. In second aquitard, the average subsidences of the clay layers located in the 71.32–92.8, 35.4–71.32 and 18.55–35.4 m below the surface are 11.91, 3.01 and 0.323 mm, respectively.

From 1984 to 2001, the compression deformation proportion of the second confined aquifer with the depth from 92.80 to 107.80 m reaches 12.45% and the subsidence of the unit thickness is 5.29 mm, which demonstrate that the compression deformation of this sandy aquifer cannot be ignored. In addition, the accumulative compression deformation proportion of the third confined aquifer whose water level depth from the surface is from 117.65 to 143.6 m is 21.34%. Its accumulative compaction deformation from 1995 to 2003 is 44.03 mm, which is the maximum compaction deformation in the aquifer system. This clearly indicates that the compressibility of the sandy layers should not be ignored.

From the preliminary analysis of the short series data from the other four extensometers, it can be also concluded that the main compaction layers are the aquifers and soft soil strata above the bottom of the third confined aquifer, and the compaction deformation of the sandy layers should not be ignored. (Because of the length limitation, the data of the other four extensometers are not listed here.) Furthermore, from the field borehole construction of the four extensometers in the 2000s, the gathered sandy cores in second confined aquifer have been consolidated in cylinder, which are quite different from the cores gotten in 1970s and 1980s.

The analysis above indicates again that the subsidence in Su-Xi-Chang area is the result of the consolidation of the sandy and soft soil strata due to the long-time excessive groundwater pumping of the confined aquifers. The subsidence is determined by not only the compressibility of aquitards, but also that of the aquifers.

Special features of individual layer deformation

The following context will focus on the special features of individual layer deformation. Here, we still take F0 extensometer for an example. Figure 8 shows the time histories (from 1990 to 2003) of deformation for individual soil stratum. Figure 8 provides the variation of groundwater level for three confined aquifers during the same period. It indicates that the groundwater level of the confined aquifers is affected by the exploitation greatly and with little seasonal disciplinarian. Because the extensometer locates in the center of the groundwater level depression cone, the deformation of the soil strata located in the extensometer have special features. Figures 8 and 9 are listed together to further elaborate the mechanism of land subsidence in this region by the curves of compression deformation of the strata versus the effective stress change (transferred from the change of groundwater level in aquifer). The deformation features of these strata are discussed below.

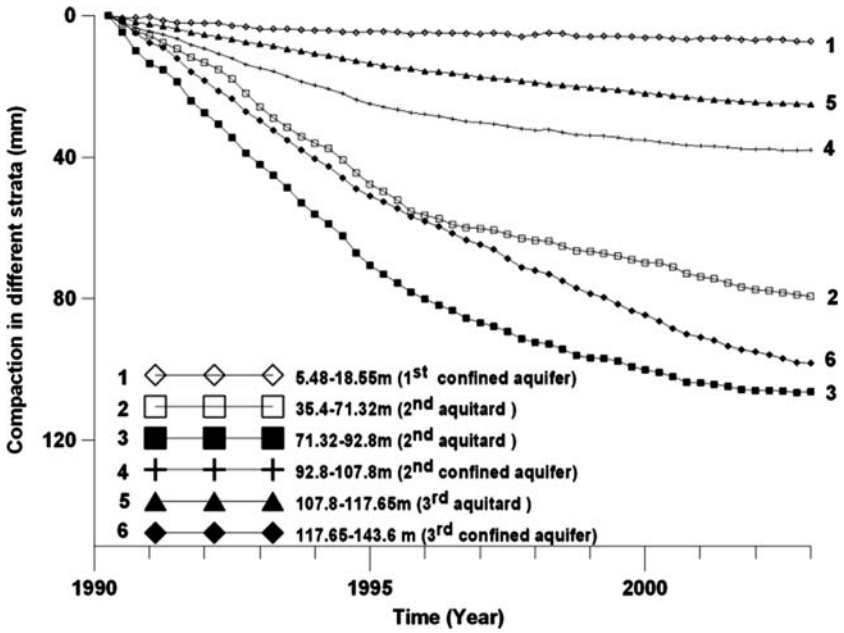

Fig. 8 Time histories of deformation for individual soil stratum of F0 extensometer

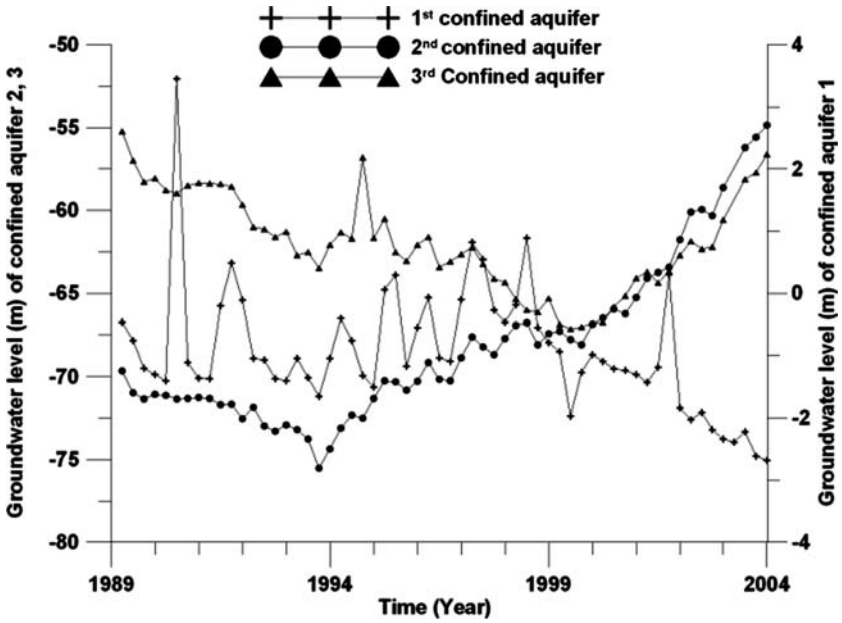

Fig. 9 Time histories of groundwater level for three confined aquifers where F0 extensometer located

Unconfined aquifer

The unconfined aquifer is mainly composed of silt clay, mingled with silt soil and fine sand silt locally. The unconfined aquifer has not been pumped yet and its level is stable yearly. The elevation of the groundwater level is about 2–4 m. The effective stress of the soil repeats increasing and decreasing in a certain scope as the level changes. The deformation of the unconfined aquifer is synchronous with the variation of the water level. When the level rises, the soil stratum rebounds, and vice versa. Generally, the deformation of the soil stratum is elastic, with little plastic deformation (as illustrated in the Fig. 10). This result is consistent with the previous traditional view that the deformation of the sandy layer is instantaneous elastic.

First and second confined aquifer

The first confined aquifer is made up of the fine sand and the fine-medium sand. The second confined aquifer is distributed in the whole area and consists of fine sand, fine-medium sand and the medium-coarse sand with gravel. As the features of these two aquifers are similar, the second confined aquifer having the larger deformation is selected to demonstrate. Figure 11 is

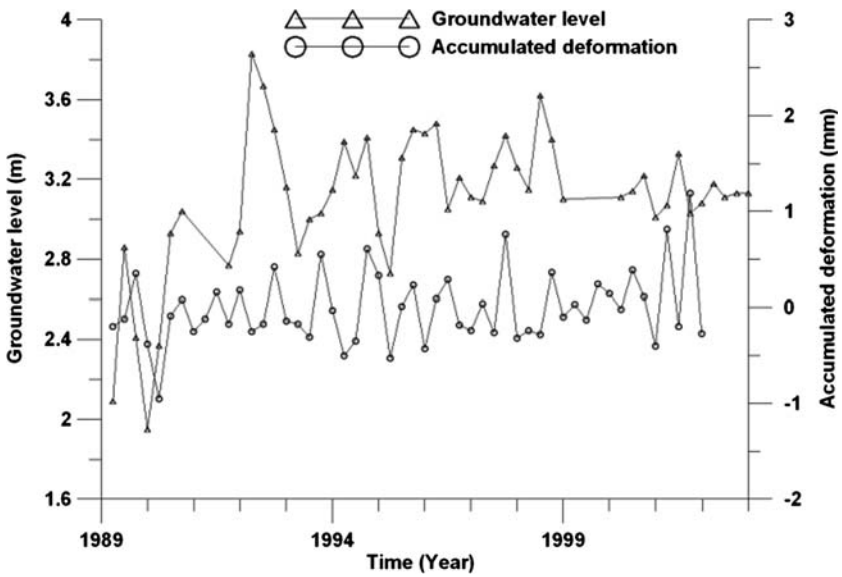

Fig. 10 Time histories of groundwater level versus accumulated deformation for unconfined aquifer

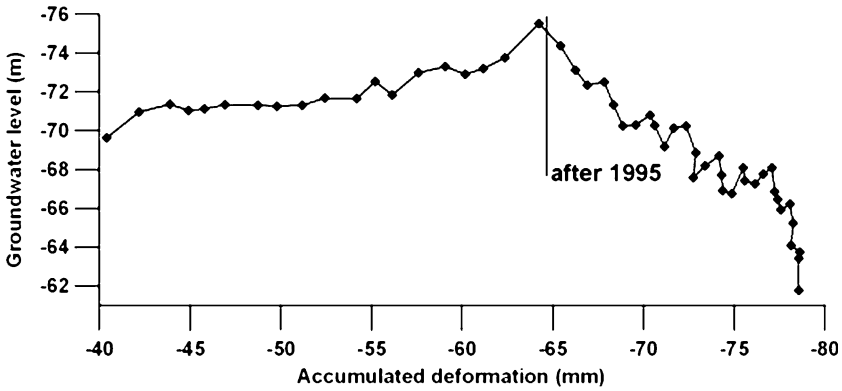

Fig. 11 Deformation of the second confined aquifer versus groundwater level from 1990 to 2003

the curve of deformation of the second confined aquifer versus the groundwater level from 1990 to 2003. The second confined aquifer is the main pumping layer in Changzhou City. Since the middle of the 1960s, the yield kept increasing. The groundwater level depth from the surface in the center of the depression cone was 20 m in the 1960s and dropped to 83.3 m in 1994. After the pumping limit in 1995, the groundwater level in the second confined aquifer in Changzhou rose gradually and the groundwater level in the F0 extensometer rose to –58.63 m in 2003. However, Fig. 11 indicates that the soil continues compacting even after 1995. Thus, it can be inferred that the lag of the deformation exists. In the traditional view, the deformation of the sandy layer is instantaneous elastic and there is no lag phenomenon. The lag phenomenon usually occurred in the soft clay layer or the permeable aquifer with interbeds because the clay layer has low permeability and the dissipation of pore-water pressure within the strata takes a long time (Leake 1990; Sneed and Galloway 2000). However, the aquifer, in the location of the F0 extensometer, is mainly composed of sand. The thickness of the aquifer is 15.0 m and its hydraulic conductivity is about 5.8×10^{-3} cm/s. From the view of the granularity constitution, the sand grain is principal, silt is next and the clay content is less than 5%. The components of clay in the whole aquifer are demonstrated in Fig. 6. Therefore, the lag phenomenon is not related with the time-dependent drainage and compaction of the interbeds in the second confined aquifer, but seems to be related with the special feature of the sandy layer.

Second aquitard

The second aquitard is distributed widely in Su-Xi-Chang area and is mainly composed of clay and silt clay. Its deformation is mainly controlled by the variation of the second confined aquifer below. Figures 12 and 13 plot the compression deformation of the two strata of second aquitard versus the change of groundwater level in second confined aquifer. The deformation feature of the second aquitard is similar with that of the second confined aquifer and the lag phenomenon is also obvious. The total compaction of the second aquitard from1990 to 2003 is 185.58 mm and the strain is 2.50%. In the same period the strain of the second confined aquifer is 2.53%.

Third confined aquifer

The third confined aquifer is mostly distributed in the northern Changzhou and the east of Suzhou. The aquifer primarily consists of fine sand silt, fine sand,

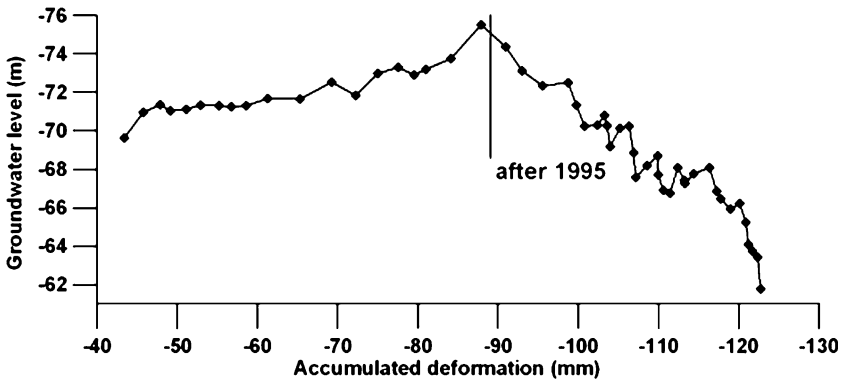

Fig. 12 Deformation of the second aquitard (39.19–71.48 m) versus groundwater level from 1990 to 2003

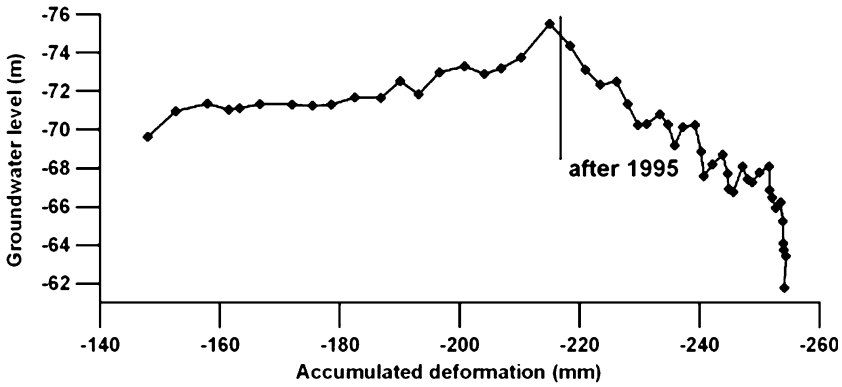

Fig. 13 Deformation of the second aquitard (71.48–92.66 m) versus groundwater level from 1990 to 2003

medium-coarse sand and fine clay particles or interbeds locally. Although the aquifer is not the main pumping layer in Su-Xi-Chang area, the groundwater level variation is similar with that of the second confined aquifer, as illustrated in the Fig. 9. The reasons are the exploitation of the third confined aquifer and the leakage supply to the second confined aquifer because of its large yield. After 1995, the yield in the whole area declined and the groundwater level of the second confined aquifer increased gradually. While the groundwater level of the third confined aquifer did not rise until 2000 because of the continuous leakage supply to the second confined aquifer. Figure 14 presents the relation of deformation of the third confined aquifer versus the groundwater level. During the fluctuation of the groundwater level, the aquifers continued compressing though its groundwater level began to rise gradually after 2000, and the deformation lag phenomenon also exists. From the analysis of clay content in the aquifer as demonstrated in Fig. 6, the sand in the aquifer is mingled with small clay particles or interbeds. Thus changes the compaction feature and results in the traditionally viewed lag phenomena (Leake 1990; Sneed and Galloway 2000).

From the above discussion, it shows that because the extensometer locates in the center of the groundwater level depression cone, the groundwater level of the confined aquifers continually declined, which caused the corresponding effective stress kept exceeding the preconsolidation stress, therefore, the deformation of the soil strata exhibited the above special features. Notably, the lag of the deformation of the sandy aquifer is common instead of specific. The hydrodynamic consolidation theory (Terzaghi 1925; Lambe and Whitman 1979) may explain the time-delay effect of subsidence in clay layers and aquifers with the low-permeability fine-grained silts, clays or interbeds such as the third confined aqufier. But, it cannot explain this situation in the sandy layer, such as second confined aquifer here. Hence, it is necessary to use other methods to investigate the mechanism of the lag phenomenon, especially that of the second confined aquifer.

Laboratory tests

In the above section, it is found that the lag phenomenon occurred in both aquifers and aquitards. Gu and Ran (2000) and Men (1999a, b) studied the creep properties of soft clay layers in the land subsidence in Shanghai and concluded that the remarkable creep of the clay layers is the other reason for lag phenomenon besides the hydrodynamic consolidation. Referring to

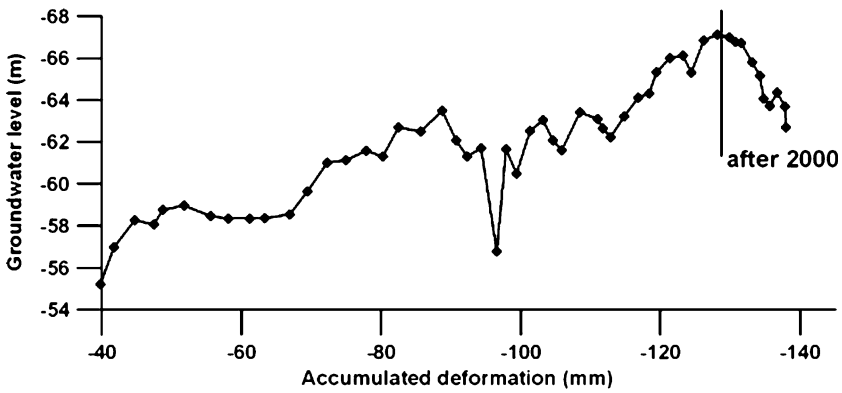

Fig. 14 Deformation of the third confined aquifer versus groundwater level from 1990 to 2003

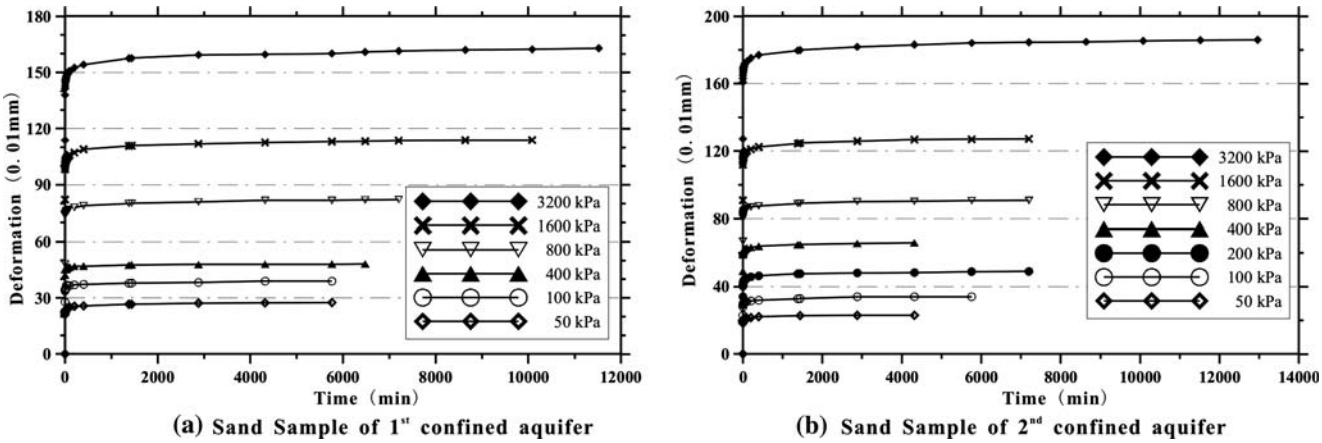

Fig. 15 The uniaxial creep curves of the sand samples in the first and second confined aquifers

the above method, in order to investigate the mechanism of the lag phenomenon in aquifers, the saturated samples (including silt clay and sand) in the aquifer system of Changzhou are obtained to study the creep behavior. The uniaxial creep tests are completed in the controlled temperature.

The uniaxial tests use the high-pressure consolidation apparatus. The samples are cylinders with a cross-section of 30 cm^2 and 2 cm high. The samples are satured before loading through different saturation methods for clay and sand sample. Different from the normal consolidation tests, every load in the experiments discussed in this paper lasted 6–10 days until the deformation becomes steady. When the deformation increment is less than 0.005 mm/day, it is regarded as stabilization.

Figure 15 is the creep curves of the sand samples from the first and second confined aquifer; Fig. 16 is that of the clay sample from second aquitard. These figures show that although the creep deformation and the time needed to be steady of sand are much less

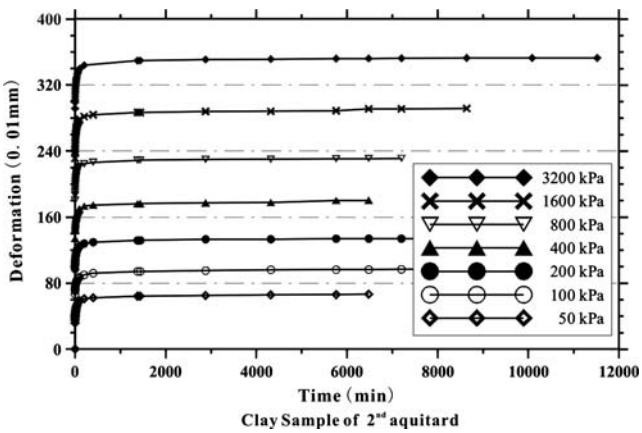

Fig. 16 The uniaxial creep curves of the clay samples in the second aquitard

than those of clay, the noticeable creep feature of sand still occurs. For sand and clay samples, the ratio of the creep deformation to the total deformation in every load is 0.08–0.17 and 0.14–0.41, respectively. Figure 17 is the isochronal curves of corresponding sand samples. The strain–stress curves are similar in the different load, which present the obvious nonlinear feature. All the results from the experiments indicate that the strain–stress–time curves of the sand samples are nonlinear and have the creep feature just as the clay sample. The creep deformation is one of the reasons for the lag phenomenon of the second aquitard besides of the drainage consolidation of the aquitard.

Note that because the clay particle content of the first and second confined aquifers in Changzhou is not high, the rheological feature of the sand samples, revealed in the experiment results, is related with its own feature, instead of having connections with the clay particle content. Table 1 lists the granularity analysis of the samples. This conclusion is not consistent with the previous opinions that the deformation of sand stratum is elastic or elastio-plastic. The creep behavior of the sand is a reasonable explanation on the lag phenomenon of second confined aquifer in Changzhou. As illuminated in the Fig. 11, the slowness of the drop and rise of the groundwater level gives the creep deformation enough time to develop. Thus, even if the rebound deformation has occurred in the sandy aquifer, it is counteracted by the creep deformation. So no rebound deformation was observed when the groundwater level increased. As a result, the aquifer keeps compressing on whole, only the subsidence rate of sandy layer deduced temporarily.

There are still questions that need to explain why the deformation of the unconfined aquifer did not have the feature of lag phenomenon: Does the unconfined aquifer have the creep feature? How about

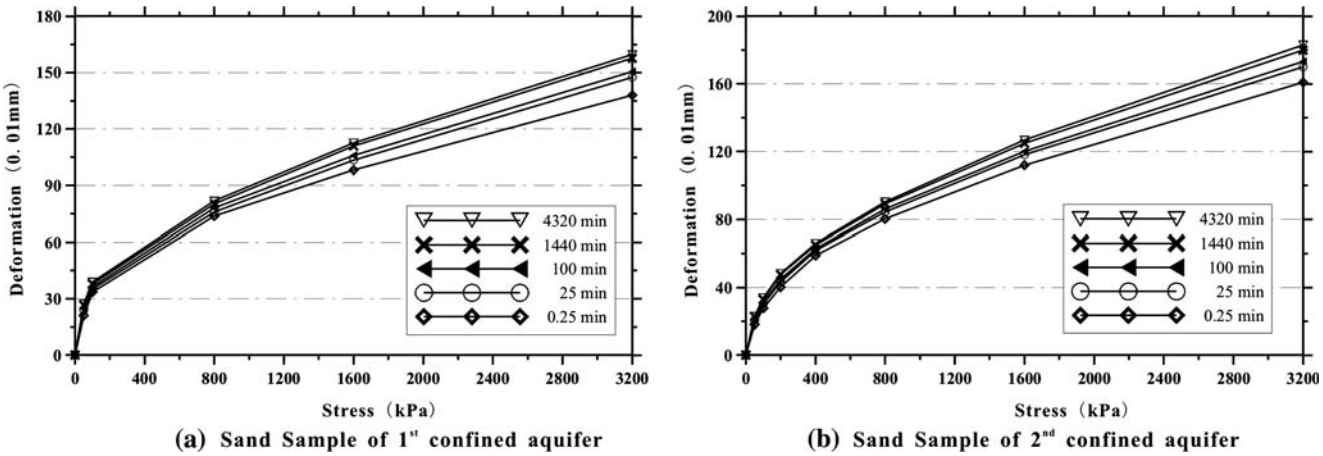

Fig. 17 The isochronal curves of the sand samples in the firs and second confined aquifers

Table 1 Granularity analyses of the creep experiment samples in the Changzhou aquifer system

Sample description	Layer	Granularity constitution (%) (grain size unit: mm)				
		>0.25	0.25–0.075	0.075–0.05	0.05–0.01	<0.01
Fine sand	First confined aquifer		77	17.9	4.2	0.9
Caesious fine sand	Second confined aquifer	18	74.3	5.1	1.3	1.3
Caesious silty clay	Second aquitard		3.0	7.5	39.5	50.0

the deformation feature of the soil strata in the brim of the groundwater depression cone?

Because the unconfined aquifer and the confined aquifers in the brim of the groundwater depression cone usually have the stable groundwater level, the effective stress of the soil repeats increasing and decreasing in a certain scope. The repeated loading–unloading unixial creep experiments are conducted to simulate the feature of the aquifer deformation. The result demonstrates that the compaction and the rebound during the loading and unloading processes are very close after two to three times of loading–unloading in a certain scope, as shown in the Fig. 18. The creep deformation and the time needed to be stable reduce gradually with the increase of the times of the repeated loading, which is the reasonable explanation for the elastic deformation of the unconfined aquifer. It is believed that the similar soil stratum in different location (the center or the brim of the groundwater depression cone) have different deformation features because of the different groundwater level fluctuation experienced.

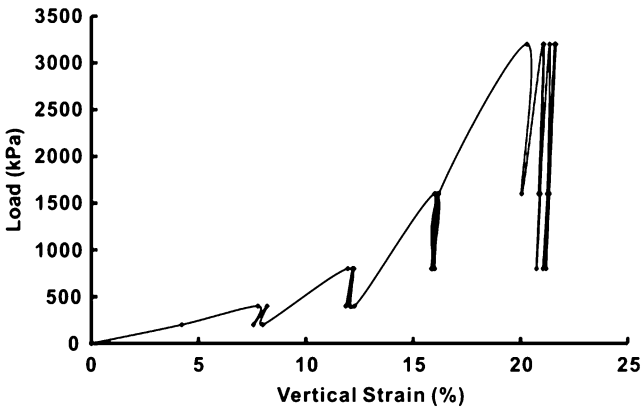

Fig. 18 The curve of stage-loading and stage-unloading tests

Creep model for saturated sand

Based on the uniaxial compression test results, the relationship of stress–strain–time for saturated sands is obtained. Plotting the strain–time curves on the log-normal coordinates $(\log \varepsilon - \log t)$, as in Fig. 19, the experimental points for all the creep curves almost fall on the straight lines. The correlative coefficients are between 0.937 and 0.998, which are larger than the corresponding ones on the single logarithmic coordinate $(\varepsilon - \log t)$. It indicates that the strain–time curves could be presented as follows:

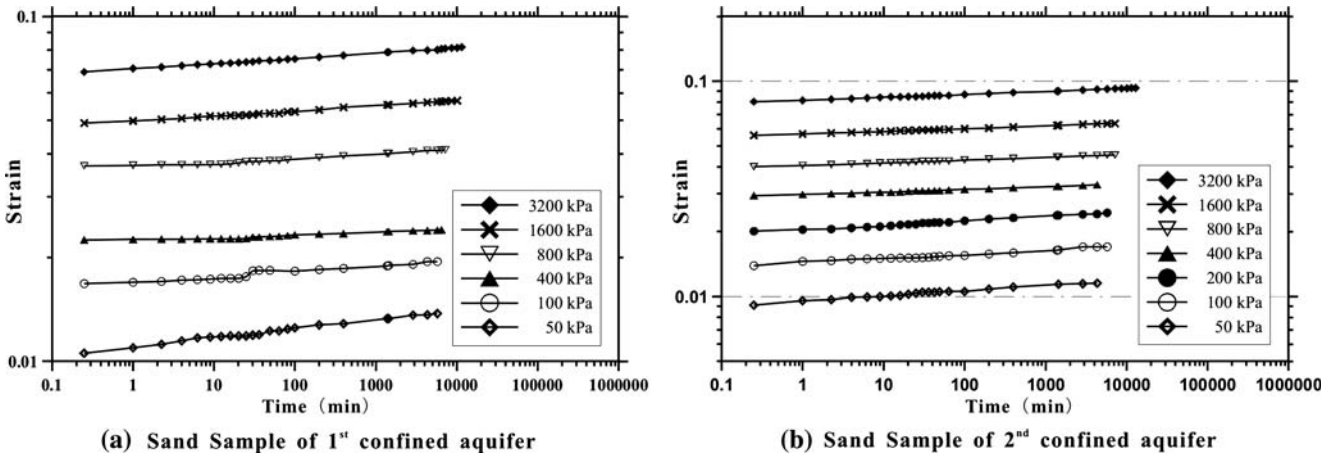

Fig. 19 The strain–time curves on the log–log coordinates of the first and second confined aquifers

$$\ln \varepsilon(\sigma, t) - \ln \varepsilon(\sigma, t_0) = m(\ln t - \ln t_0) \quad (1)$$

Rearranging Eq. 1 gives,

$$\varepsilon(\sigma, t) = \varepsilon(\sigma, t_0)\left(\frac{t}{t_0}\right)^m \quad (t>0) \quad (2)$$

where t_0 is reference time, which could be taken as 1 min; $\varepsilon(\sigma,\ t)$ is the strain under the pressure σ at t moment; $\varepsilon(\sigma,\ t_0)$ is the instantaneous strain under the pressure σ at t_0 moment; t is time; m is the slope of the straight lines, which is related with the soil property. For an identical soil sample, the straight lines are almost paralleled, which indicated that the parameter m could be a constant.

In the same way, plotting the isochrones on the $\log \sigma - \varepsilon$ and $\log \sigma - \log \varepsilon$ coordinates, respectively, it is also found that the strain–stress curves are almost the straight lines on $\log \sigma - \log \varepsilon$ coordinate (as shown in Fig. 20). The correlative coefficients are between 0.937 and 0.998, which are larger than the corresponding ones (usually 0.91–0.93) on the single logarithmic coordinate ($\log \sigma - \varepsilon$). As a result, the strain–stress relationship could be presented in the following form:

$$\ln \varepsilon(\sigma, t) - \ln \varepsilon(\sigma_0, t) = n(\ln \sigma - \ln \sigma_0) \quad (3)$$

Rearranging Eq. 3 gives,

$$\varepsilon(\sigma, t) = \varepsilon(\sigma_0, t)\left(\frac{\sigma}{\sigma_0}\right)^n \quad (4)$$

where σ_0 is reference pressure, which could be taken as 100 kPa; $\varepsilon(\sigma_0,\ t)$ is the instantaneous strain under the pressure σ_0 at t moment; n is the slope of the straight lines. For an identical soil sample, the parameter n could be treated as a constant, despite the little fluctuation. Taking the sample from the first confined aquifer as an example, the parameter n decreased from 0.447 to 0.401 corresponding to the time changing from 1 min to 96 h.

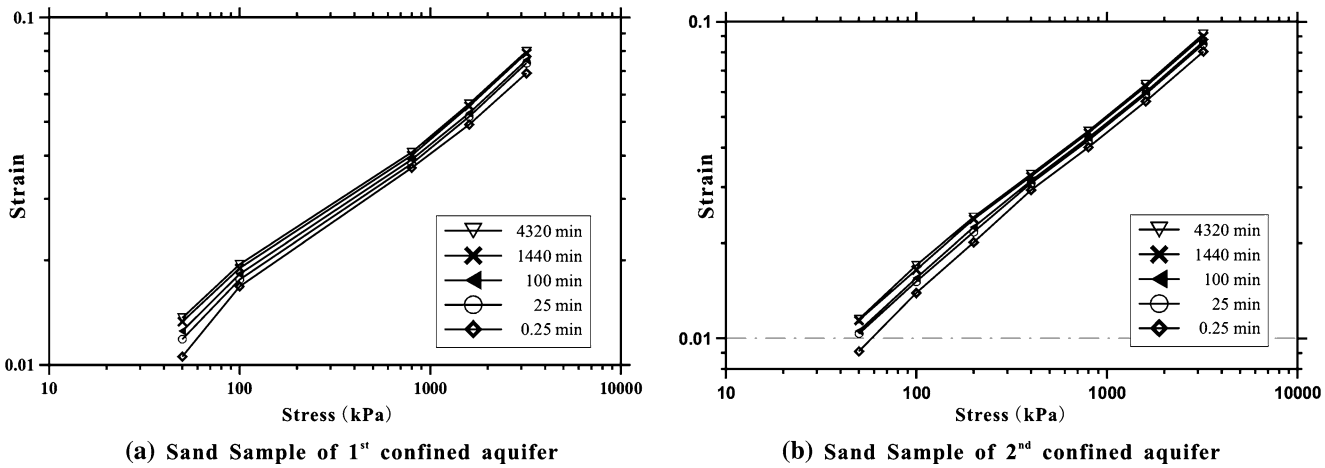

Fig. 20 The strain–stress curves on the log–log coordinates of the first and second confined aquifer

Similarly, the relationship between $\varepsilon(\sigma, t_0)$ and stress σ at $t = 0$ could be fitted by straight lines on the log–log coordinate. As a result, it gives:

$$\varepsilon(\sigma, 0) = \varepsilon(\sigma_0, 0)\left(\frac{\sigma}{\sigma_0}\right)^n \tag{5}$$

where $\varepsilon(\sigma, 0)$ and $\varepsilon(\sigma_0, 0)$ is the instantaneous strain under the pressure σ and σ_0, respectively.

Based on Eqs. 2 and 4, we could get:

$$\varepsilon(\sigma, t) = \varepsilon(\sigma_0, t_0)\left(\frac{t}{t_0}\right)^m\left(\frac{\sigma}{\sigma_0}\right)^n \tag{6}$$

where $\varepsilon(\sigma_0, t_0)$ is the strain under the pressure σ_0 at t_0 moment, which is fixed for a certain soil samples; m is the slope of the creep curves on the log–log coordinate and is a dimensionless parameter.

Defining $A = \varepsilon(\sigma_0, t_0)$, rewriting Eq. 6 to obtain the nonlinear creep model for saturated sand,

$$\varepsilon(\sigma, t) = A\left(\frac{t}{t_0}\right)^m\left(\frac{\sigma}{\sigma_0}\right)^n \quad (t>0) \tag{7}$$

There are three parameters A, m and n in this model. All the parameters have the clear physical meanings and could be easily gotten from experiments. A is obtained from the corresponding 1 min strain in the creep curve on the 100 kPa pressure. Plotting the creep curves and the isochrones on the log–log coordinate, respectively, the slopes of the corresponding fitted straight lines are the value of m and n. Based on the experimental data, the fit parameters for sand samples in Changzhou confined aquifers are listed in Table 2.

The strain in the Eq. 7 is the total strain under the pressure σ. It includes the instantaneous strain and the creep strain, which increases with the time. In order to clarify the creep deformation, the strain rate is obtained by differentiating the Eq. 7 with respect to t:

$$\dot{\varepsilon}(\sigma, t) = A\frac{m}{t_0}\left(\frac{t}{t_0}\right)^{m-1}\left(\frac{\sigma}{\sigma_0}\right)^n \tag{8}$$

The instantaneous deformation does not change with the time, so actually the Eq. 8 presents the creep deformation. The experiment results indicate the m is the less than 1, which implies that the creep rate decreases with the time. The relationship between the creep rate and the time in the log–log coordinate is linear, which is in accordance with the conclusion in the Singh–Mitchell creep model (Singh and Mitchell 1968). The sand creep feature is related with the slip in the interface of the grain (Vyalov 1986; Poul and Liu 1998; Prisco et al. 2000). There exists different size of pores between the sand particles, which are in the balanced condition. The shear–stress on the particles' interface increases under the load. The particles move along the interface and into the bigger pores. After the filling of the bigger pores, the space becomes small, the shearing resistance increases and the move velocity decreases. Therefore, the sand particles need time to be in a new balance. From the macro view, the whole process presents that the deformation of the sand increases with time until stabilization.

Table 2 Creep parameters for sands of Changzhou

Samples	A	m	n
First confined aquifer	0.0170	0.0154	0.4217
Second confined aquifer	0.0146	0.0164	0.4972

Conclusions

Based on the analysis of the experiment results and the monitoring field data, including extensometer groups and observation wells in Su-Xi-Chang area, the following conclusions could be drawn:

1. The occurrence and the development of the land subsidence in Su-Xi-Chang area are in close relationship with the groundwater pumping both in time and space. The configuration of the subsidence cone is basically identical with shape of the groundwater depression cone.
2. The consolidation of the sandy layers and the compaction of the neighboring clay layers contribute most of land subsidence. The main consolidation layers are the soft mud layers; however, the compressibility of the confined sandy layers should not be ignored. The second, third confined aquifers contributed more than 30% of the total subsidence from 1984 to 2001. The field observation data indicate, although the groundwater level rose slowly after 1995, all the layers including the sandy layers continued compacting in less quantity. The lag of the deformation of the sandy layers is common instead of specific.
3. It is traditionally recognized that the deformation of sandy layer is elastic. However, because of the complicated geological condition in field, the sand in the aquifer is perhaps mingled with small clay particles or interbeds, which will change the traditional view of the instantaneous compaction feature in the pure sandy aquifer and result in the

lag phenomena. The monitoring field data of Su-Xi-Chang area revealed that the sand has creep feature, which is another important reason for the lag phenomenon in the sandy layer deformation except the sand composition (mingled with small clay particles or interbeds). Based on the laboratory tests results, the relationship of stress–strain–time for saturated sands is obtained; and it could be expressed as power functions. The test results also show that the strains for sands depend not only on the stresses exerted on them but also the time elapsed. That is to say that the sands have characteristics of nonlinear creep. The creep behavior of the sand may be attributed to the movement of the sand particles.

4. The complexity of both the soil formation and the fluctuation of the groundwater level determine the complicated deformation of the soil stratum. Different sandy layers deform diversely under different stress conditions. The soil strata, including both sandy layers and clayey layers, located in the center of the groundwater level depression cone exhibited obvious viscous mechanical behavior because of the slowness and continuance of the groundwater level drop. However, for the sandy layer after a period of stabilization or increase of the groundwater level, the creep deformation becomes stable and exhibits elastic feature. When establishing land subsidence model for the similar soil stratum, the deformation could be elastic, visco-elastic and even elastic–visco-plastic because of the different groundwater level fluctuation experienced.

Acknowledgments The author would like to express appreciation to the two anonymous reviewers for their valuable comments and suggestions. This paper is financially supported by the National Nature Science Foundation of China grants 40335045 and 40402023.

References

Gambolati G, Freeze RA (1973) Mathematical simulation of the subsidence of Venice: 1. Theory. Water Resour Res 9(3):721–733

Gambolati G, Gatto P, Freeze R A (1974) Mathematical simulation of the subsidence of Venice: 2. Results. Water Resour Res 10(3):563–577

Gu XY, Ran QQ (2000) A 3-D coupled model with consideration of rheological properties. Land subsidence. In: Proceedings of the 6th international symposium on land subsidence, vol 11, pp 355–365

Helm DC (1975) One-dimensional simulation of aquifer system compaction near Pixley, California, (1) constant parameters. Water Resour Res 11:198–212

Helm DC (1976) One-dimensional simulation of aquifer system compaction near Pixley, California, (2) stress-dependent parameters. Water Resour Res 12:121–130

Hu RL, Wang SJ, Lee CF, Li ML (2002) Characteristics and trends of land subsidence in Tanggu, Tianjin, China. Bull Eng Geol Environ 61(3):213–225

Lambe TW, Whitman RV (1979) Soil mechanics. SI version. Wiley, New York

Leake SA (1990) Interbed storage changes and compaction in models of regional groundwater flow. Water Resour Res 26(9):1939–1950

LEHGGS (Laboratory of Engineering and Hydrological Geology and Geophysical Survey, Liege university, Belgium, Institute of geological survey of Belgium), GCSER (Geological center of Shanghai Economic Region) (1989) Study on the quaternary geology, hydrogeology, engineering geology and mathematical model of land subsidence of Yangtze Delta of Shanghai (in Chinese)

Liu CH, Pan YW, Liao JJ, Huang CT, Shoung OY (2004) Characterization of land subsidence in the Choshui River Alluvial Fan, Taiwan. Environ Geol 45(8):1154–1166

Men FL (1999a) Preliminary investigations on rheological properties of clay and ground settlement in Shanghai City (I) (in Chinese). J Nat Disasters 8(3):117–126

Men FL (1999b) Preliminary investigations on rheological properties of clay and ground settlement in Shanghai City (II) (in Chinese). J Nat Disasters 8(4):123–132

Pratt WE, Johnson DW (1926) Local subsidence of the Goose Creek field. J Geol 34(7):577

Prisco D, Imposimato S, Vardoulakis I (2000) Mechanical modeling of drained creep triaxial tests on loose sand. Geotechnique 50(1):73–82

Poland JF, Davis GH (1969) Land subsidence due to withdrawal of fluids. In: Reviews in engineering geology, vol II. Geological Society of America, p 187

Poul VL, Liu CT (1998) Experimental study of drained creep behavior of sand. J Eng Mech 124(8):912–920

Sneed M, Galloway DL (2000) Aquifer-system compaction and land subsidence: measurements, analyses, and simulations-the Holly Site, Edwards Air Force Base, Antelope Valley, California. US Geological Survey Water-Resources Investigations Report 00–4015, pp 65

Singh A, Mitchell JK (1968) General stress–strain–time function for soils. J Soil Mech Found Div ASCE 194(1):21–46

Terzaghi K (1925) Erdbaumechanik auf bodenphysikalisher Grundlage. Deuticke, Wien

Vyalov SS (1986) Rheological fundamentals of soil mechanics. Translated by Sapunov OK. Elsevier, Amsterdam

USGS (1999) Land subsidence in the United States. In: Galloway D, Jones D, Ingebritsen SE (eds) Circular 1182. ASCE, New York, pp 177

Yu J, Wu JQ, Wang XM, Yu Q (2004) Research on the correlative prediction model with a regional decomposition base of the land subsidence in the Suzhou-Wuxi-Changzhou area (in Chinese). Hydrogeol Eng Geol 4:92–95